Allostery in Rabbit Pyruvate Kinase: Development of A Strategy To Elucidate the Mechanism †

ARTICLE *in* BIOCHEMISTRY · DECEMBER 1998

Impact Factor: 3.02 · DOI: 10.1021/bi981273y · Source: PubMed

4 AUTHORS, INCLUDING:

Robert H E Friesen
Janssen Pharmaceuticals Inc
29 PUBLICATIONS **1,687** CITATIONS
SEE PROFILE

James Ching Lee
University of Texas Medical Branch at Galves…
140 PUBLICATIONS **5,679** CITATIONS
SEE PROFILE

Werner Braun
University of Texas Medical Branch at Galves…
145 PUBLICATIONS **11,215** CITATIONS
SEE PROFILE

Allostery in Rabbit Pyruvate Kinase: Development of A Strategy To Elucidate the Mechanism†

Robert H. E. Friesen,‡ Regis J. Castellani,§ J. Ching Lee,* and Werner Braun*

Sealy Center for Structural Biology, Department of Human Biological Chemistry and Genetics, The University of Texas Medical Branch at Galveston, Galveston, Texas 77555-1157

Received May 28, 1998; Revised Manuscript Received August 28, 1998

ABSTRACT: Isozymes of pyruvate kinase (PK) expressed in rabbit muscle and kidney show different allosteric kinetics. The only amino acid changes in the two isozymes, originating from alternative RNA splicing, occur at a stretch of 55 amino acids in the C domain near the subunit interface. The self-correcting distance geometry (SECODG) program DIAMOD was used to calculate a homology model of these interfacial contacts in the four helix bundle of the kidney PK dimer, based on the X-ray structure of the tetrameric rabbit muscle PK [Larsen et al. (1994) *Biochemistry 33*, 6301−6309]. Energy refinement with the program FANTOM, using the ECEPP/2 force field to assess packing and electrostatic interactions between the two subunits, yielded two groups of energetically favorable conformations. The primary difference in the two groups is the loop conformation of residue Pro 402, which is serine in muscle PK. In one loop conformation, the conserved Lys 421 can form an intersubunit salt bridge as observed in the muscle PK crystal structure. The other loop conformation favors an alternative intrasubunit salt bridge, similar to that found in the *Escherichia coli* PK structure, which was not used for generating the model. The intersubunit salt bridge leads to an intersubunit hydrogen bonding between Lys 421 of one subunit and Tyr 443 of the other. To provide direct evidence on the roles of these residues, site-directed mutagenesis of the muscle PK gene was conducted. Converting Ser 402 to a proline and Tyr 443 to a phenylalanine changed neither the secondary nor the tetrameric structure, as measured by far UV-CD and sedimentation velocity, respectively. However, the S402P mutant exhibits steady-state kinetics, indicating that the mutant is more reponsive to regulation by effectors, while the mutant Y443F was essentially equivalent to wild-type muscle PK protein except for a lower affinity to phosphoenolpyruvate. These findings suggest a pivotal role for a few key residues in the allosteric regulation in PK.

Allosteric mechanisms are essential in the regulation of metabolism, intercellular communication, gene expression, and other cellular functions. One of the central issues in allostery is the mechanism(s) of signal transmission. Are the allosteric signals transmitted through pathways specific for each signal or are the binding sites of allosteric effectors connected in a global manner? A mechanism involving specific pathways implies that the protein molecule consists of modules, which can be used in designing a novel protein with a priori specified allosteric properties. However, a global mechanism would complicate the engineering process. The long-term goal of our study is to elucidate the general mechanism of conferring allostery and to identify the structural elements involved. The system chosen is the mammalian pyruvate kinase (PK),[1] a central enzyme of cellular glycolysis. The unique feature of this system is the existence of two isozymic forms which exhibit very different regulatory patterns, but their primary sequences of 530 amino acids differ only by 22 residues localized in an intersubunit interface (*1*−*8*). The fact that a 4% change in sequence can exhibit such a drastic impact on the regulatory behavior on this key glycolytic enzyme implies that there is a good chance to accomplish the long-term goal of this study.

While M_1-PK is the major form in tissues such as muscle, where glycolysis predominates, the M_2-PK isozyme is found in tissues such as kidney, where gluconeogenesis plays a

† The computation study was supported by NSF Grant DBI-9714937, DOE Grant DE-FG03-96ER62267 and John Sealy Memorial Endowment Fund for Biomedical Research Grant 2573-97 to W.B.R.H.E.F. and R.C., who contributed equally, were supported by NIH Grant GM-45579 and Robert A. Welch Foundation Grants H-0013 and H-1238 to J.C.L.

* To whom correspondence should be addressed. Phone: (409) 747-6810. Fax: (409) 747-6850. E-mail: werner@nmr.utmb.edu.

‡ Present address: Department of Microbiology, University of Groningen, Kerklaan 30, g751 NN Haren, The Netherlands.

§ Residence Rifo-Rhone, Avenue des Freres Lumiere, 13500 Martigues, France.

[1] Abbreviations: buffer A, 20 mM Tris-base, 100 mM KCl, 15% (v/v) glycerol, 1 mM DTT, 0.2 mM FBP, 0.1 mM EDTA, and 0.1 mM phenylmethanesulfonyl fluoride, pH 7.9; buffer B, 5 mM KP_i, 1 mM EDTA, 1 mM DTT, 0.2 mM FBP, 5 mM $MgSO_4$, and 100 mM KCl, pH 7.5; buffer C, same as buffer B with no KCl and at pH 6.0; DTT, dithiothreitol (Cleland's reagent); EDTA, ethylenediaminetetraacetic acid; FBP, fructose, 1,6-bisphosphate; IPTG, isopropyl β-D-thiogalactoside; MWC, Monod−Wyman−Changeux; PEP, phosphoenolpyruvate; Phe, L-phenylalanine; PK, pyruvate kinase; R and T states, active and low-active states; RKPK, rabbit kidney pyruvate kinase; RMPK, rabbit muscle pyruvate kinase; RMSD, root-mean-square deviation; SECODG, self-correcting distance geometry; TKM buffer, 50 mM Tris, 72 mM KCL, and 7.2 mM $MgSO_4$, pH 7.5; TKMD buffer, 50 mM Tris, 72 mM KCL, 7.2 mM $MgSO_4$, and 0.2 mM DTT, pH 7.5; DIAMOD, distance geometry application for modeling; FANTOM, fast Newton−Raphson Torsion angle minimizer; ECEPP, empirical conformational energy for peptides and proteins.

10.1021/bi981273y CCC: $15.00
Published on Web 10/16/1998

significant role. They are products of alternative splicing of the same gene. Out of a total of 530 residues, the only difference between these two isozymes resides in a stretch of 55 residues, encoded by an exon (*7*). Out of these 55 residues, 22 are different. In contrast to the small sequence difference, the thermodynamic and kinetic properties of the two isozymes are dramatically different. M_1-PK exhibits hyperbolic Michaelis−Menten kinetics whereas M_2-PK shows sigmoidal behavior (*6*, *8*). The concentrations of effectors to which these isozymes respond are millimolar and micromolar for M_1- and M_2-PK, respectively. M_1-PK is a stable tetramer while M_2-PK undergoes a dimer ⇌ tetramer reversible association, the equilibrium of which is dependent on the presence of effectors.

Muscle PK is the best characterized PK isozyme with respect to both structure and functional behavior. Crystal structures of rabbit muscle PK (RMPK) (*1*) and cat muscle PK (*2*, *3*) have been determined and refined at 2.9 and 2.6 Å resolution, respectively. The M_1-type isozyme consists of four subunits of 530 residues, each of which contains four domains designated as N-terminal (1−42): A (43−115 and 224−387); B (116−223); and C (388−530). The four subunits of RMPK form two different subunit interfaces. The 1,3 subunit interface involves intersubunit contacts of domains A and C, and the 1,2 subunit interface involves mainly intersubunit contacts of domain C. The active site lies in the pocket between domains A and B of the same subunit and is far removed from these subunit interfaces.

The three-dimensional structure of the M_2-type PK (RKPK) has not been determined, hence, structural rationale for the difference in kinetic and biophysical behavior between the two isozymes is not available. Nevertheless, progress in molecular modeling programs such as DIAMOD[2] (*9*−*11*) and the energy refinement and Monte Carlo simulation programs such as FANTOM[2] (*12*−*15*) enables one to rationally identify those residues among the 22 possible substitutions which significantly perturb the structure and/or the noncovalent network of interactions. In addition with the availability of both the RMPK and RKPK genes in overexpression plasmids (*4*, *5*), we can test the effect of individual sequence substitutions between these isozymes on the kinetics and use the 3D model to connect the structural perturbation at the subunit interface to the active-site region. Specifically, we examine what are the neighboring side chains that interact with the substituted residue and how would a substitution affect this network of noncovalent interactions?

In this study, a strategy is developed and its validity tested. The strategy consists of (a) computational chemistry to sample low-energy conformations of the interfacial region of RKPK and compare these structures with the RMPK structure; (b) the residues identified by both sequence difference and computation as to significantly perturb the structure will be the target sites for mutation studies; (c) the individual contributions of these residues will be tested using mutants derived from site directed mutagenesis; and (d) the validity of the proposed disturbance in the network interactions involving the residue under investigation in point c will be tested with further mutagenesis which may involve residues that are conserved between the two isozymes.

[2] The programs DIAMOD and FANTOM are available on request from W. Braun.

Using the strategy, residues 402 and 443 were studied. Residue 402 is identified by both sequence difference and computation while residue 443 is an application of step (d) of the strategy. The results indicate that both residues play key roles in conferring allostery in mammalian pyruvate kinase and the strategy should be further developed while the X-ray crystallographic structures of these mutants are being determined.

MATERIAL AND METHODS

Materials. Lactate dehydrogenase, disodium salt of ADP, phosphoenolpyruvate, Tris base, and Tris-HCl were purchased from Boehringer Mannheim. Reduced nicotinamide adenine dinucleotide (NADH), L-phenylalanine (Phe), potassium chloride, sodium chloride, and phenylmethanesulfonyl fluoride (PMSF) were all obtained from Sigma Biochemicals. Mono- and dibasic potassium phosphate were purchased from Fisher. [^{35}S]dATPαS was purchased from Amersham Life Science. Oligonucleotides were purchased from Genosys Biotechnologies, Inc.

Molecular Modeling. The modeled region is the α1-loop-α2 motif, residues 388−423, which upon association of two RMPK subunits, forms an antiparallel four-helix bundle (*1*, *3*, *6*, *17*). Distance geometry calculations in torsion angle space (*18*) were performed with the program DIAMOD (*15*), a version of the program DIANA (*9*) which includes a SECODG method (*10*). Starting with 50 random coils with the appropriate RMPK or RKPK sequence, DIAMOD generates an ensemble of 50-folds. The two chains of subunits 1 and 2 were linked with a chain of 64 pseudo amino acids from residue 423 (backbone carboxy carbon) of the subunit 1 to 388 (backbone nitrogen) of subunit 2 to define the relative position and orientation of the two chains. The ψ, ϕ dihedral angles and $C^{\alpha}-C^{\alpha}$, $C^{\beta}-C^{\beta}$ distances were extracted from the RMPK crystal structure (*1*) with the program Cofima. The constraints of the ψ, ϕ dihedral angles were applied on all residues except on Ala 401−Pro 402 in the RKPK and Ser 401−Ser 402 in the RMPK, where the steric clash inherent to the Pro and X-Pro residue conformation could not satisfy the dihedral angle values of Ser 401 and Ser 402 in the RMPK. In addition, χ^1 dihedral angles on the helical segments (residue 390−400 and 408−421) were restrained to a value between −240 and 0 for Phe, Tyr, His, Arg, Met, Glu, and Gln and between −240 and −120 for Val. These values are fulfilled in 95% of α-helices in globular proteins (*19*). In the DIAMOD calculations, the 2849 $C^{\alpha}-C^{\alpha}$ and $C^{\beta}-C^{\beta}$ distances for residues 388−400 and 403−423 separated by at least three residues were used for the RMPK calculation and 3184 distance constraints were used for RKPK. The conjugate gradient algorithm minimizes the target function consisting of a hard-sphere potential representing the size of the atoms and the angle and distance constraints by gradually increasing the minimization level so that, at first, only interactions between neighboring residues are considered and, at the end, interactions between all residues (*20*). The weight factors chosen emphasize the van der Waals contact contribution on the target function over the constraint term. In DIAMOD (*15*), distance constraints are gradually included during minimization in several steps. The number of these steps was 30 and the total number of iterations was 23 200 for both proteins.

Structures generated by DIAMOD were refined with FANTOM (*12*), a torsion angle minimizer with an efficient Newton−Raphson algorithm. The ECEPP/2 force field (*21*) was used, and the maximum number of iterations was set to 300 steps. A distance-dependent dielectric constant was employed with an 8 Å cutoff, and the nonbonded pair list was updated every 10 minimization steps. In the FANTOM calculations, the constraints on the C^{β} atoms were discarded to allow greater sampling of the side-chain conformations. The number of $C^{\alpha}-C^{\alpha}$ distance constraints were 923 for both proteins. These distance constraints were included with a low weight by adding a violation of 5 Å as a energy contribution of $kT/2$ to the total potential energy ($k = 1.987$ cal/mol/K and $T = 298$ K). Dihedral angle restraints were also relaxed in the energy refinement.

All calculations were performed on an Silicon Graphics Indigo 2 workstation with a R8000 processor and 192 Mb of RAM and a Cray J-90 with four processors and 256 Mb of RAM in the Sealy Center for Structural Biology.

Evaluation of the Model. The quality of the model structure was evaluated by calculating the root-mean-square deviation (RMSD) of the RKPK backbone atoms from the RMPK with the program COMPAR. The solvent-accessible surface of the structural motifs was calculated with the program ANAREA (*15*). Stereochemical analysis was performed with the program Procheck (*22*), the following parameters were estimated and compared with the expected values derived from high-resolution protein structures: (i) main-chain bond length and bond angles, (ii) peptide ω angles, (iii) Cα tetrahedral distortion, (iv) φ, ϕ Ramachandran plots, and (v) nonbonded close contacts.

Site-Directed Mutagenesis. The mutagenic oligonucleotides used for constructing the specific point mutants are as follows:

Mutant S402P: GCGCGAGCCTCCCCTCACTCCACAGAC
AG

Mutant Y443F: CAAGTGGCCCGGTTCCGCCCGCGC
A

The underlined sequences are the mutagenic nucleotides with the corresponding wild-type sequence underneath. Mutagenesis of the PK gene was performed directly with the double-stranded plasmid containing the RMPK gene using the same procedure established by Cheng et al. (*4*). Two oligonucleotide primers, a mutagenic and a selection primer, were simultaneously annealed to one strand of the denatured plasmid. Wild-type plasmids, containing an intact *Nde*I restriction site, could be linearized while mutant plasmids were selected by its resistance to digestion. The reaction mixture was transformed into JM109 cells. Plasmids were isolated from culture of individual transformants and screened by *Nde*I digestion.

DNA sequencing of double-stranded DNA was performed by the dideoxynucleotide chain termination method of Sanger et al. (*23*) using Sequenase Version 2.0 (United States Biochemicals).

Overexpression of Wild-Type RMPK and RMPK Mutants. *E. coli* JM109 cells containing the plasmid were grown and harvested under the same conditions established by Cheng et al. (*4*).

Protein Purification and Preparation. Wild-type and mutant RMPK were purified by a previously published procedure (*4*). The procedure consists of polyethyleneimine and $(NH_4)_2SO_4$ precipitation steps which are followed by Superdex-200 and SP-Sepharose chromatography. The only exception in the current procedure is the inclusion of 0.2 mM FBP and 0.1 mM EDTA instead of β-merceptoethanol in both buffer A and B. The purified protein was precipitated with 70% ammonium sulfate and stored at 4 °C. The protein concentration was determined by absorbance at 280 nm, using an absorptivity of 0.54 mL/mg cm (*24*).

Enzyme Kinetics. The enzymatic activity of RKPK was determined by the lactate dehydrogenase coupled enzyme assay (*25*) in a buffer consisting of 50 mM Tris base, 72 mM KCl, 7.2 mM $MgSO_4$, and 0.3 mM NADH and 10 μg/mL lactate dehydrogenase and varying amount of Phe and FBP as indicated. The final concentration of ADP or PEP in the assay mixture was fixed at 2 and 1 mM, respectively, while varying the concentration of the other substrate. After adjusting the pH of the assay mix to 7.5 at 23 °C, LDH equilibrated with TKM buffer was added, and the assay mix was finally brought to the desired volume. The reaction was started by the addition of 0.15 μg of Y443F or 0.10 μg of S402P in 3 μL of TKMD to 1 mL of assay solution that had been equilibrated at 23 °C. The decrease in absorption at 340 nm was followed as a function of time with a Hitachi U-2000 spectrophotometer to obtain ν, the observed steady-state kinetic velocity. All data sets were fitted to the modified version of Hill equation as shown in equ 1 (*26*):

$$\nu = \frac{V_{max}[S]^n}{K_{app}^n + [S]^n} \quad (1)$$

where V_{max} is the maximal velocity of each data set, [S] is the concentration of the variable substrate, n is the Hill coefficient, and K_{app} is a complex steady-state kinetic equilibrium constant that is equivalent to the K_m in the Michaelis−Menten equation where $n = 1$.

SDS−Gel Electrophoresis. SDS−10% polyacrylamide gel electrophoresis was performed according to the method of Laemmli (*27*), followed by staining with Coomassie Blue. The markers used for molecular mass weight determination were phosphorylase b (97 400 Da); bovine serum albumin (66 200 Da); ovalbumin (45 000 Da); carbonic anhydrase (31 000 Da).

Circular Dichroism. CD spectra of wild-type RMPK, S402P RMPK, and Y443F RMPK were measured with an Aviv 62 DS circular dichroism spectrometer. Solutions with concentrations of 0.5 mg/mL were measured in a fused quartz cuvette with a path length of 0.1 cm. Each spectrum was recorded with a 0.5 nm increment and 1 s intervals. For each sample, three repetitive scans were obtained and averaged.

Velocity Sedimentation. Velocity sedimentation experiments were performed in a Beckman Optima XL-A analytical ultracentrifuge (Palo Alto, CA) with an An-60Ti rotor, equipped with absorption optics. The experiments were carried out at 30 000 rpm at 23 °C, and data were collected at 280 nm in the continuous mode with a radial stepsize of 0.003 cm, 8 min intervals. Data were collected on 400 μL samples loaded into double sector centerpieces. Weight

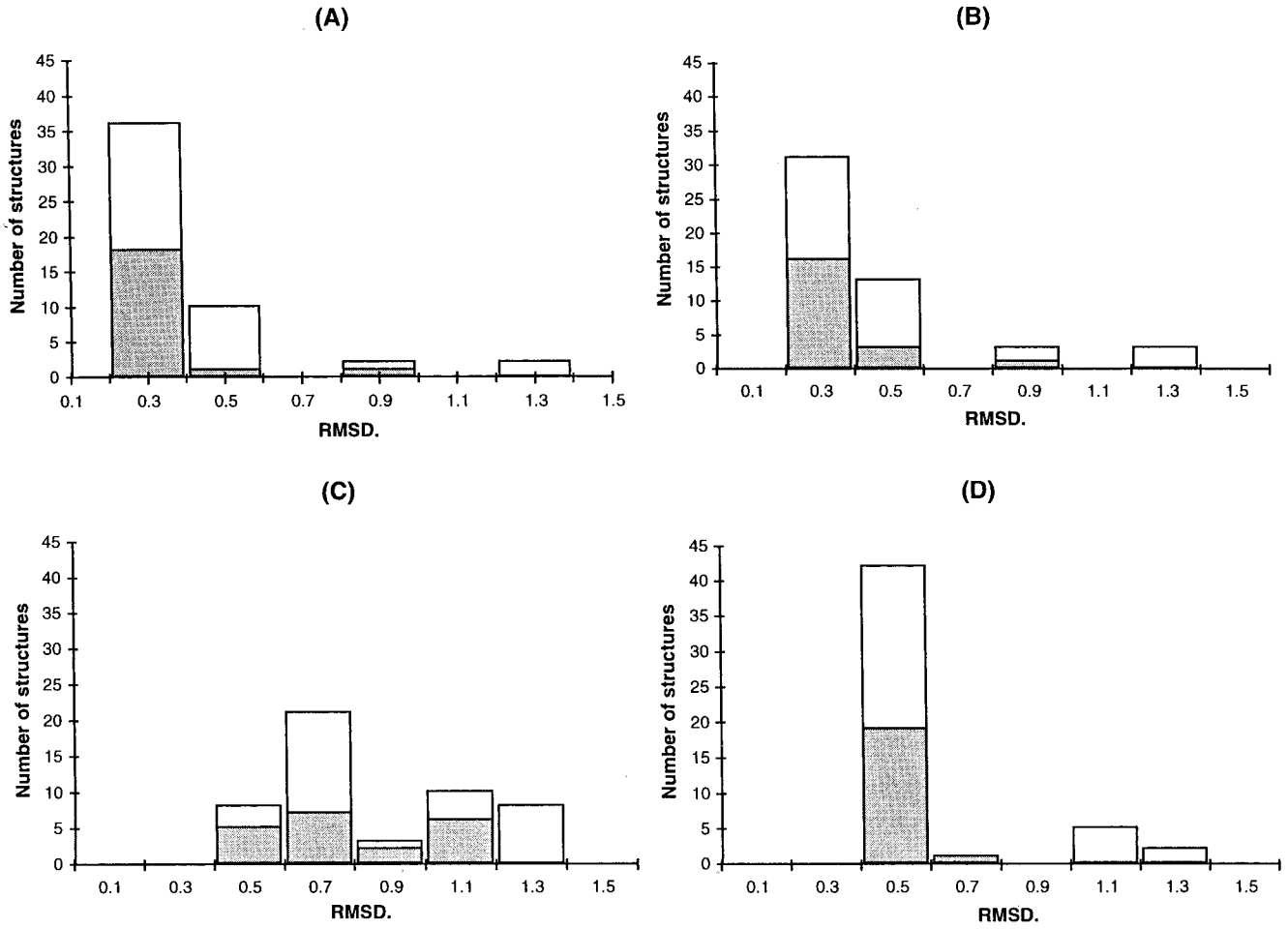

FIGURE 1: Distribution of RMSDs of the loop (residues 400−408) of the 50 structures predicted with DIAMOD for (A) RMPK chain A, (B) RMPK chain B, (C) RKPK chain A, (D) RKPK chain B. Each of the structures were superimposed with the RMPK crystal structure (*1*) on all backbone atoms of the loop region between the two helices α1 and α2 and the RMSD of these atoms were calculated. Hatched areas show the distribution of the 10 structures with the lowest target function.

average sedimentation coefficients were obtained by employing the Beckman data analysis software.

RESULTS

Conformational Sampling of RMPK and RKPK by SECODG Calculations and FANTOM Energy Refinement. Distance and dihedral angle constraints defining the dimer of the helix-loop-helix motif comprising the regions which include residues 388−423 of subunit 1 and subunit 2 were extracted from the X-ray crystal structure of RMPK (*1*). Ensembles of 50 conformations satisfying these and hard-sphere steric constraints were calculated by the SECODG program DIAMOD for the RMPK and RKPK sequences. Initial structures for both sets of calculations were random coils so as to achieve widespread sampling of loop conformations and of side-chain conformations at the subunit interface. We wanted to sample conformations of the interface region of RKPK with low energy and to compare these structural perturbations with those found in the RMKP sequence. Thus, the differences in these perturbations are due to the sequence difference and not due to the constraints.

The range of residual target function values for the ensemble of 50 structures is 2.8−4.3 Å^2 for RMPK and 4−13 Å^2 for RKPK. The low target function values demonstrate that the RKPK sequence is compatible with the 3D structure of RMPK. The main differences between the structures are in the loop region defined by residues 401−408. The RMSD analysis of the backbone atoms of the loop (Figure 1) indicates alternative loop conformations whose deviations from the X-ray crystal structure of RMPK are more pronounced for the RKPK than the RMPK structures. Whereas the RMSD values for the bulk of the muscle structures are low (0.3−0.5 Å; Figure 1, panels A and B), those for the kidney structures are significantly higher with a biphasic distribution (Figure 1, panels C and D). Some RKPK structures still have loop conformations similar to the X-ray crystal structure of RMPK with RMSD values of about 0.5 Å, but a sizable fraction of structures have different loop conformations with RMSD values exceeding 1 Å.

Each DIAMOD structure was further refined with restrained energy minimization using the ECEPP/2 semiempirical force field implemented in FANTOM. All energy contributions were substantially reduced in the restrained energy refinement (Table 1). The individual energy terms were reduced with a dominant decrease in the Lennard-Jones energy of about 750 kcal/mol in RMPK and 600 kcal/mol in RKPK. The torsional energy contribution is the same in both ensembles indicating no difference in strain of the structures. The Lennard-Jones potential in the RMPK is lower by about 20 kcal/mol, indicating a tighter hydrophobic

Table 1: Energy Refinement[a] of the 50 DIAMOD Structures of RMPK and RKPK by FANTOM

structures	E_{conf}[b] (kcal/mol)	E_{el}[c] (kcal/mol)	E_{HB}[d] (kcal/mol)	E_{LJ}[e] (kcal/mol)	E_{tor}[f] (kcal/mol)
RMPK					
initial	625 ± 333	204 ± 22	-31 ± 13	270 ± 329	182 ± 8
final	-595 ± 30	-59 ± 26	-130 ± 5	-489 ± 13	83 ± 6
RKPK					
initial	386 ± 65	125 ± 21	-38 ± 16	135 ± 50	164 ± 6
final	-584 ± 25	-87 ± 26	-113 ± 3	-461 ± 12	77 ± 7

[a] Mean values and standard deviations of the total conformational energy and of individual contributions are given. [b] Total ECEPP/2 energy. [c] Electrostatic energy. [d] Hydrogen bond energy. [e] Lennard-Jones energy. [f] Torsional energy.

packing in the RMPK structures. The final conformational energies of the RKPK bundle are comparable to those of the RMPK sequence within the standard deviations. The large decrease of the total conformational energy was achieved with only slight increase in the restrained energy term by about 5 kcal/mol for both proteins.

The Procheck analysis (*22*) confirmed the stereochemical quality of all five low-energy conformations for the muscle and kidney PK. In the Ramachandran plot, 98.5−100% of all residues in the energy refined structures for RMPK occupied the core and the allowed regions. The backbone dihedral angle ϕ and ψ for all residues in the RKPK structures were completely within these regions. No bad contacts were observed, and the overall rating of the structures was class 1 or 2 in the Procheck classification scheme (*28*).

The RMSD distributions of the loop conformations in the two ensembles of energy-refined structures (Figure 2) are broader than in the ensembles after SECODG calculations alone (Figure 1). The uniform distribution for the RMPK structures, as compared to biphasic grouping for the RKPK structures, can still be seen, indicating alternative loop conformations in the latter.

Alternative Loop and Side-Chain Conformations in RKPK. An outstanding feature of the conformation of the loop is the solvent-accessible surface of Lys 421 which is reduced by 150 Å^2 upon subunit association in the RMPK X-ray structure. This is the largest change in the accessible surface areas among all residues in the helix-loop-helix motif of RMPK when compared to that in the single subunit. The five conformers in each ensemble in the RKPK structures with the lowest potential energy were chosen for more detailed analysis. The extensive intra- and intersubunit contact of Lys 421 to other side chains in the modeled region was determined. In one of the conformers, Lys 421 can form hydrogen bonds to the carbonyl oxygens of Ser 401, Ser 404, and Glu 409 in the loop region of the other subunit (Table 2). Furthermore, an intersubunit salt bridge between Lys 421 and Glu 409 (dashed yellow line in Figure 3A) can form, the same salt-bridge interaction as in the RMPK structure. These distances are listed as intersubunit distances [inter-(1,2) or inter(2,1)] in Table 2. Alternatively, in the other conformer, as shown in Figure 3B, Lys 421 can form an intrasubunit salt-bridge to Glu 417, listed as intra(1,1) or intra(2,2) for the subunits 1 and 2. Short contacts indicative of side-chain interactions, i.e., distances of <3.5 Å, are given in bold face. The same pattern of salt-bridge interaction as in the RKPK structures II and V is also observed for the analogous residues in the X-ray structure of *E. coli* PK (*29*) as seen in the last line of Table 2. RKPK structures with higher energy were also seen where both Lys 421s were involved in intrasubunit salt bridges (data nor shown).

All five low-energy conformers of RMPK have the same intersubunit contacts of Lys 421 to the loop region as the X-ray crystal structure of RMPK. The large distances of Nζ of Lys 421 to the side-chain oxygen of Glu 417 within the same subunit show the absence of any intrasubunit salt bridges in these five structures.

The primary feature of the alternative loop conformations is the Pro 402 position, which is nested within the groove formed by the loop of the residues defined by the C-terminus of helix α1 and the N-terminus of helix α2 in the C domain. When proline is outside the loop, Lys 421 can form the intersubunit contact to Glu 409 as seen in the RMPK structure. Presumably due to steric hindrance, when proline is turned inward, the Lys 421 side chain swings back toward its own subunit and participates in a salt-bridge network with Glu 417.

Possible Linkage between Lys 421 and Active Site. The subunit interface region near Lys 421 is quite remote from the binding site of pyruvate in the RMPK structure (Figure 4). Proximal residues, Arg 442 and Tyr 443, strongly conserved in the PK family, are possible interaction partners for the carboxy terminal end of the α-helix Aα6. This helix spans the length of a PK subunit ($\sim$30 Å). The substrate-binding site of PEP is located near the N-terminal end of this helix. Hence, helix Aα6 could serve as a link between the active site and the intersubunit interface, similar to the dynamic role of the FG corner in hemoglobin which transmits conformational changes upon ligand binding at the heme group to the $\alpha-\beta$ interface region (*30*).

The importance of many of the residues implicated in the interaction (amino acids 398, 402, 409, 417, 421, and 443) is indicated by their high degree of primary sequence conservation when comparing the PK isozymes from various organisms (*31*). Lys 421 is conserved in all mammalian PKs and *E. coli* type 1 PK, although a small group of PKs contain the positively charged Arg at this position. Residues Glu 417 and Tyr 443 are strictly conserved in all known PKs and Glu 409 is conserved in all but two PKs where it is replaced by the negatively charged Asp.

Construction, Overexpression, and Purification of RMPK Mutants. Two point mutations, S402P and Y443F, were introduced into RMPK, and both mutants were structurally and functionally characterized. The choice of S402P is dictated by the natural sequence difference between RMPK and RKPK, which shows a proline replacing a serine at residue 402 (*5*) and the computation results implicating the role of P402 in the formation of alternate loop conformations. The choice of Y443F mutation is to test the hypothesis derived from computation that K421 forms an intersubunit H bonding with Y443 and salt bridge with E409. The Y $\rightarrow$ F represents the minimum perturbation of this intersubunit network. Mutations were confirmed by DNA sequencing of the constructed plasmids. Mutant proteins were overexpressed and purified from *E. coli* as described for wild-type RMPK (*4*) except for addition of 0.2 mM dithiothreitol (DTT) and 0.4 mM fructose 1,6-bisphosphate (FBP) to all purification buffers to stabilize the mutants. Both mutants eluted from the gel-filtration and cation-exchange column

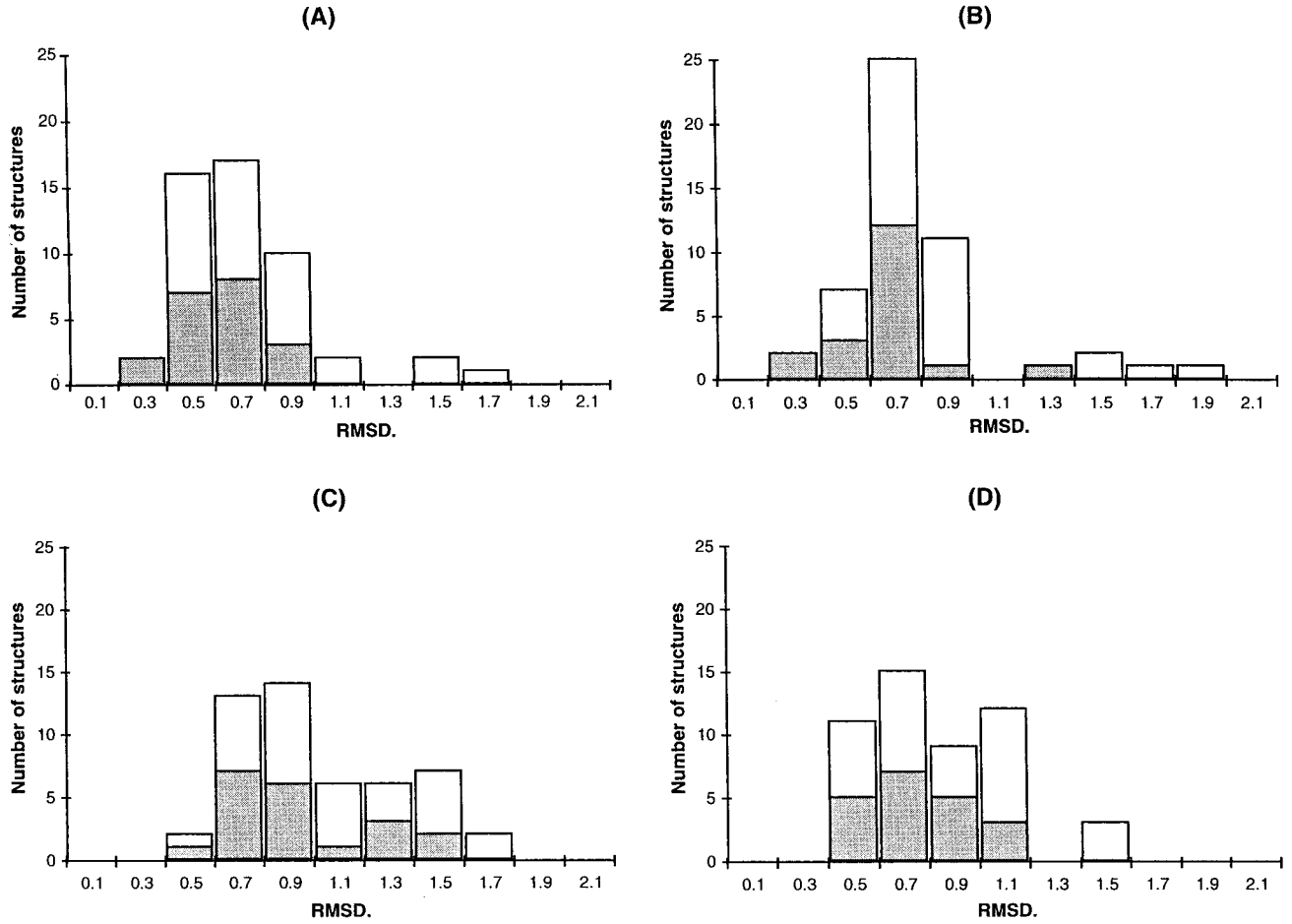

FIGURE 2: Distribution of RMSDs of the loop (residues 400−408) of the 50 structures energy refined with FANTOM for (A) RMPK chain A, (B) RMPK chain B, (C) RKPK chain A, (D) RKPK chain B, as described in the legend of Figure 1. Hatched areas show the distribution of the 10 energy refined structures with the lowest target function.

at the same position as that of wild-type RMPK. This indicates that wild-type and mutant RMPKs have similar surface charge distribution. The S402P and Y443F mutants were purified to greater than 97% homogeneity as examined by SDS−PAGE stained by Coomassie Blue with yields of 10.2 and 1.2 mg/L of culture, respectively.

Biophysical Characterization of RMPK Mutants. The secondary structures of the S402P and Y443F mutants were monitored by far-UV-CD and compared to wild-type RMPK (Figure 5). The far-UV spectra of S402P and wild-type RMPK are identical. The spectrum of the Y443F mutant is consistently lower over the full range (260−290 nm). However, when the data are transformed to molar ellipticity by adjusting for protein concentration and the lowered molar absorptivity of the Y443F mutant, it is clear that neither mutation caused major secondary structural changes. These results imply that the wild-type and mutant RMPKs are folded into a similar motif.

The quaternary structure of the wild-type and RMPK mutants were monitored by sedimentation velocity. Weight average sedimentation coefficients of mutant and wild-type RMPK were determined at different protein concentrations at pH 7.5 and 23 °C in TKMD buffer. A system that undergoes self-association would exhibit a concentration dependence of the weight average sedimentation coefficients. The experimentally determined sedimentation coefficients of the S402P and Y443F mutants are similar to that determined for wild-type RMPK, as shown in Table 3. Since the sedimentation coefficients were similar in a wide range of protein concentration, it can be concluded that both mutants of RMPK form stable tetramers at the experimental protein concentrations.

Kinetic Characterization of Mutant S402P and Y443F. Steady-state kinetics obtained for the S402P, Y443F, and wild-type RMPK with PEP as the variable substrate are shown in Figure 6 and with ADP as the variable substrate (data not shown). Parameters derived from these steady-state kinetic experiments are summarized in Table 4 for the PEP titrations, and in Table 5 for the ADP titrations.

It is apparent from Figure 6A that the S402P mutation results in a saturation curve intermediate to wild-type RMPK and RKPK. Analysis of the derived kinetic parameters in Table 4 confirms this observation. To study the effects of the S402P mutation in more detail, saturation curves were analyzed in the presence of the inhibitor Phe with or without FBP, which can reverse the effects of Phe. Wild-type RKPK is more sensitive than RMPK to Phe inhibition. In the presence of 2 mM Phe, the apparent affinity of RKPK for PEP is 3.0 mM with a Hill coefficient (n) of 2.3 (*5*). In the presence of 12 mM Phe, the apparent affinity of wild-type RMPK for PEP increases by a factor of 4, and n increases from 1.0 to 1.8 (*4*). The affinity of S402P for PEP increases by a factor of 29, and n increases from 1.0 to 2.6. The inhibitory effect of 12 mM Phe can be partially reversed by

Table 2: Intrasubunit and Intersubunit Interactions of Lys 421 in Five Energy Refined FANTOM Structures with Lowest Conformational Energy[a]

structures	contacts of K421				
	E_{conf}[b] (kcal/mol)	intra[b] (1,1) (Å)	inter[c] (1,2) (Å)	intra[d] (2,2) (Å)	inter[e] (2,1) (Å)
RMPK					
I	−683.5	10.2	**2.7**	8.4	**2.7**
II	−668.8	8.1	**2.7**	4.5	**2.6**
III	−651.0	12.3	**2.5**	12.4	**2.7**
IV	−647.4	8.0	**2.6**	8.1	**2.7**
V	−646.7	6.4	**2.6**	6.0	**2.5**
RKPK					
I	−646.8	9.1	**2.5**	6.0	**2.7**
II	−637.5	**2.6**	5.7	8.3	**2.7**
III	−631.0	6.2	**2.6**	5.1	**2.7**
IV	−622.7	5.3	**2.6**	10.0	**2.5**
V	−619.2	11.6	**2.6**	2.6	4.1
RMPK X-ray structure	na[g]	7.9	**2.7**	7.9	**2.7**
E. coli PK X-ray structure[f]	na	4.3	7.1	**3.2**	8.0

[a] Structures are sorted according to the total ECEPP/2 energy. Distances representing hydrogen bond or salt-bridge interactions are given in boldface. [b] Minimum distance of K421 Nζ to E417 Oϵ1 and Oϵ2 within subunit 1. [c] Minimum distance of K421 Nζ of subunit 1 to S401 O, S404 O, E409 Oϵ1, Oϵ2, and E409 O of subunit 2. [d] Minimum distances as in footnote b within subunit 2. [e] Minimum distances of K421 of subunit 2 to the loop residues, defined in footnote c, of subunit 1. [f] Ref *29*. The distances indicated were calculated for D348, K351, E356, E364, and K368 which are structural homologous to the RMPK residues S401, S404, E409, E417, and K421, respectively. [g] na, not applicable.

the presence of 10 mM FBP. The S402P mutant is more sensitive than the wild-type RMPK to Phe inhibition, although the effective concentrations of these allosteric regulators are still in millimolar similar to that of the RMPK isoform.

The apparent affinity for ADP was tested by varying the ADP concentration while keeping the concentration of PEP at 2 mM. The ADP titration of the S402P mutant is similar to that of wild-type RMPK with a minor decrease in the catalytic efficiency (Table 5).

Mutant Y443F showed a significantly different set of kinetic properties (Figure 6B). In the absence of effectors, the saturation curve of Y443F is characterized by an apparent affinity for PEP of 0.05 mM and a Hill coefficient of 1.1. The presence of 12 mM Phe shifts the saturation curve to higher PEP concentrations, resulting in a significantly increased apparent affinity for PEP of 0.66 mM and a Hill coefficient of 1.9 similar to wild-type RMPK. The inhibitory effect of 12 mM Phe can be partially reversed by the presence of 10 mM FBP. The catalytic efficiency of Y443F was decreased compared to wild-type RMPK under all studied conditions. The apparent affinity of Y443F for ADP is similar to that of wild-type RMPK except for a significant decrease in the catalytic efficiency.

DISCUSSION

Allosteric phenomenon is mediated through interfacial interactions in the form of either domain−domain or intersubunit interactions. Thus, an intriguing challenge to protein engineering is how to confer allostery via perturbation of interfacial interaction? What is the target of perturbation? Would the mutation disturb the pathway of signal transmission or does it simply alter the energetic constraints in the interfacial interaction? Before a rational scheme can be proposed for engineering desirable allosteric behavior, it is important to establish some of the ground rules that govern the observed allosteric effects. However, there is limited knowledge on allosteric systems to establish these ground rules. Even with systems with high-resolution structures to define the atomic details of interfacial interactions, additional information such as that gleaned from molecular genetics and solution biophysical chemistry is needed to reveal the molecular mechanism of allostery.

A strategy to extract this vital information from isozyme forms of mammalian PK is developed, and the usefulness of this strategy is tested. A major feature of this strategy hinges on the availability of the sequences of the two PK isozymes. The sequence differences identify the specific sites of amino acid changed and the nature of changes that are needed to confer allostery. Computational chemistry is then applied to sample major structural changes in the helix-loop-helix motif as a consequence of change in the sequence. The residue(s) most likely responsible for these major structural changes are identified. Mutants are generated and in vitro kinetic and biophysical properties of these mutants characterized so as to correlate the residues in this interfacial region of PK and the observed differences in the kinetic properties of M_1- and M_2-PK.

In vitro study of wild-type RKPK shows that all substrates and effectors communicate through this interface (*5*). Each ligand exhibits a specific thermodynamic signature, namely, PEP enhances the energetics of interfacial interaction, while ADP exhibits the opposite effect Phe or FBP binding to RKPK elicit opposite effects on the energetics of subunit assembly. Having established the pathways of communication to this subunit interface, it is then possible to address the issue of the roles of the amino acids that are different between RMPK and RKPK in conferring allostery. Do different residues control specific ligand-binding sites? Does each residue modulate the effects of other residues, and does this helix-loop-helix motif behave as an interlocked unit?

Conformational sampling of model structures of the RKPK in the interface region, based on the known X-ray structure of RMPK, suggest possible conformational changes in the RKPK. Distance geometry in torsional angle space (*10*, *15*, *18*), combined with energy minimization and Monte Carlo simulation (*12*−*15*), is particularly useful for homology modeling of structures. DIAMOD calculates three-dimensional structures of proteins with standard bond length and bond angle geometry, and the steric hindrance of all atoms is explicitly included. The resulting conformations are therefore stereochemically correct (*32*). It allows a search for alternative model structures often not found by model building procedures which map the polypeptide chain of the model sequence most closely to the 3D template structure. This method was crucial and proven to be successful in designing point mutation studies to map the binding site of the measles virus receptor CD46 (*33*, *34*). Results of molecular modeling show that the basic feature of a helix-loop-helix motif observed in muscle PK is maintained even with the 22 amino acid substitutions. However, the loop region in RKPK can apparently adopt at least two different conformations. The residue that might play a significant role

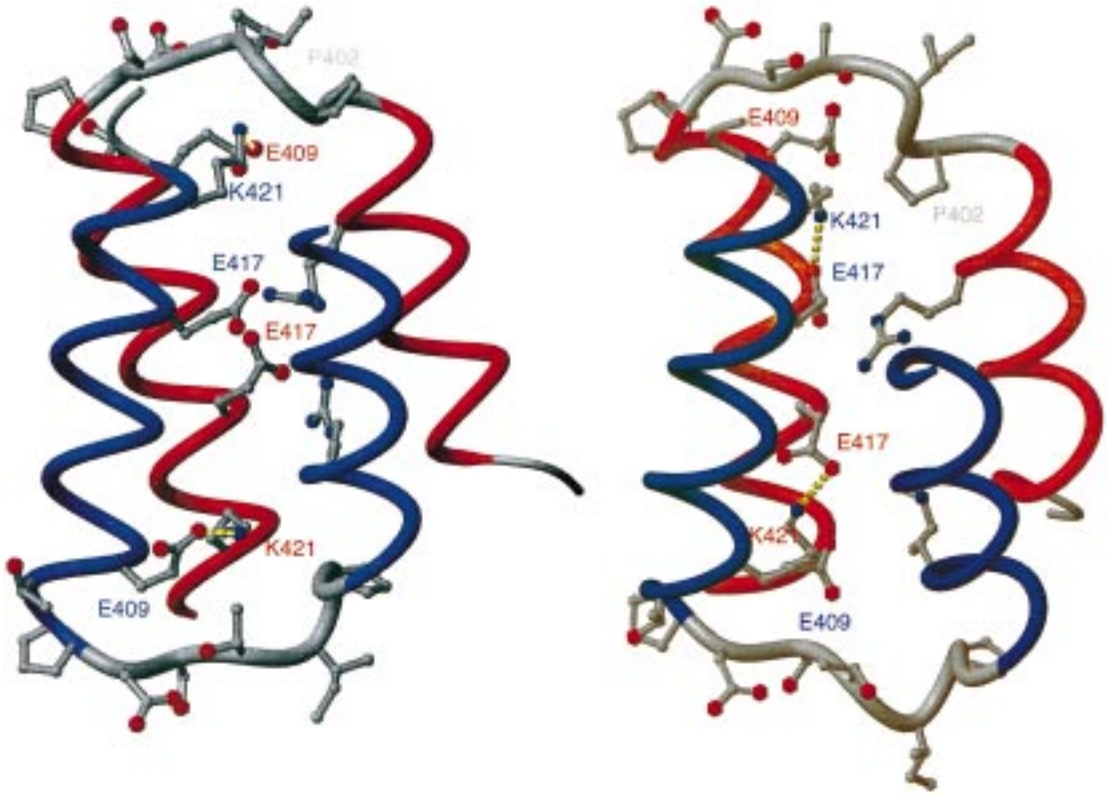

FIGURE 3: Representation of the four helix bundle formed by the α-turn-α motif of RKPK subunits 1 and 2. Helical regions are shown in red and blue for subunit 1 and 2. The loop regions are colored in gray. (A) Model PK structure similar to the RMPK crystal structure, representing structures I, III and IV of Table 2. Dotted lines outline the interaction between Lys 421 of one subunit with Glu 409 of the other subunit across the 1, 2, or 9 subunit interface. (B) Alternative PK model structure representing the structures II and V. The dotted lines show the intra subunit salt-bridge between Lys 421 and Glu 417. In contrast to the conformation shown in panel A the position of Pro 402 is located inside the loop between helix 1 and helix 2. Figure was prepared with the program MOLMOL (*35*).

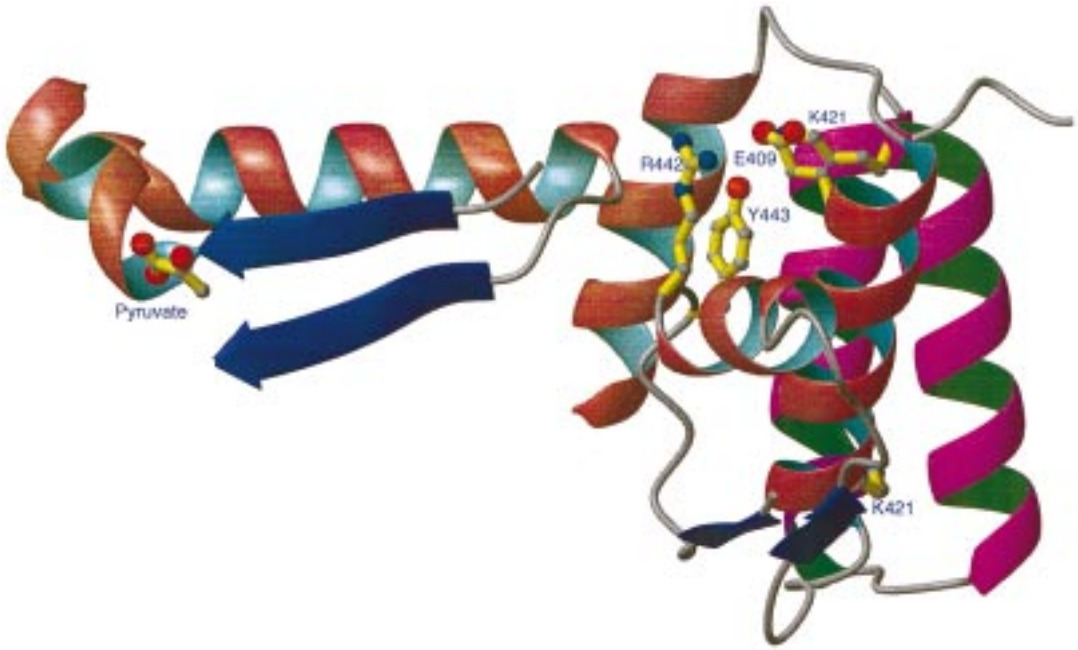

FIGURE 4: Relative position of the q interface in RMPK to the active site. Helical regions in the C domain of subunit 1 and 2 are colored pink and orange, respectively. Individual residues shown are K421, E409, R442, and Y443. Only helices Aα6 and Aα5 and the adjacent β-sheets of the A domain are shown as part of the postulated communication pathway from the interface to the active site. This representation was made with the program MOLMOL (*35*).

in defining the distribution of these conformations could be identified by the primary sequences of RMPK and RKPK. The difference in this loop region is residue 402, which is a serine in RMPK but a proline in RKPK. Accordingly, the S402P mutant of the RMPK was generated and studied. This mutant shows little conformational change and in the overall structure of the protein as monitored by CD and sedimentation velocity. The allosteric behavior of this S402P RMPK

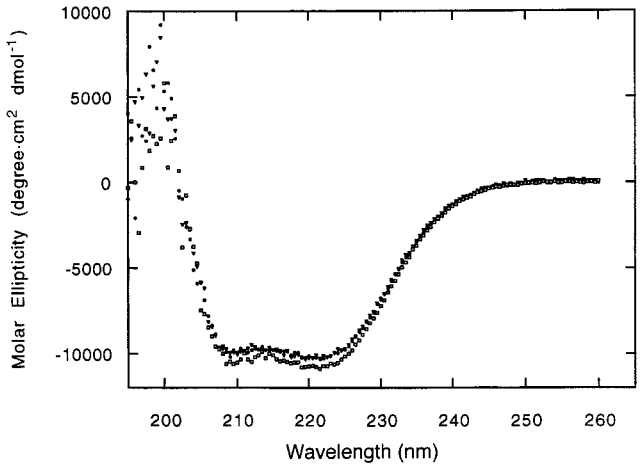

FIGURE 5: CD spectra (molar ellipticity) in the far-UV region of wild-type RMPK (○), S402P RMPK (●), and Y443F RMPK (□) in TKM buffer at 23 °C.

Table 3: Weight-Average Sedimentation Coefficients $S_{20,w}$ for Wild-Type RMPK, S402P, and Y443 Mutants at Different Protein Concentrations

PK	concentration (mg/mL)	$S_{20,w}$[a]
WT RMPK	0.485	10.1
S402P RMPK	0.05	10.0
S402P RMPK	0.75	10.3
Y443F RMPK	0.05	10.1
Y443F RMPK	0.6	9.8

[a] $S_{20,w}$ values were measured at pH 7.5 and 23 °C in TKMD buffer.

mutant indicates that this mutant is more responsive to effectors than wild-type RMPK. One of the outstanding steady-state kinetic differences between the muscle and kidney isozymes is the responsiveness of the kidney isozyme to effectors. The ratio of K_{app} for PEP in the presence and absence of Phe is used to demonstrate the change in kinetic properties induced by the S402P mutation. The ratio is about 4 and 19 for WT RMPK and RKPK, respectively, as shown in Table 4. In the S402P RMPK mutant, this ratio is about 29. Thus, these initial screening studies indicate that a single mutation dictated by the sequence difference can confer some of the kinetic features characteristic of the RKPK isozyme. These results imply that the strategy which is being developed can provide the type of information sought. Thus, it is worthwhile to employ these mutants for further indepth studies. The exact nature of perturbation induced by the S402P mutation cannot be deduced by this study alone since the mutation can affect any of the large number of equilibrium constants that govern the behavior of this enzyme. Nevertheless, the net effect is that this single mutation confers partially the allosteric behavior typically associated with RKPK.

What is the structural basis for the perturbation in the enzyme kinetics observed in the S402P mutation? The molecular model of this subunit interface of RKPK suggests a pathway for the transmission of the allosteric message from the active site of one subunit to the next subunit across the interface. In this proposed model, Lys 421 is involved in a hydrogen bond with Tyr 443 of the adjacent subunit through the groove within the loop between the two helixes and via a salt bridge with Glu 409. Tyr 443 forms part of a hydrogen bond network responsible for the transmission of the signal.

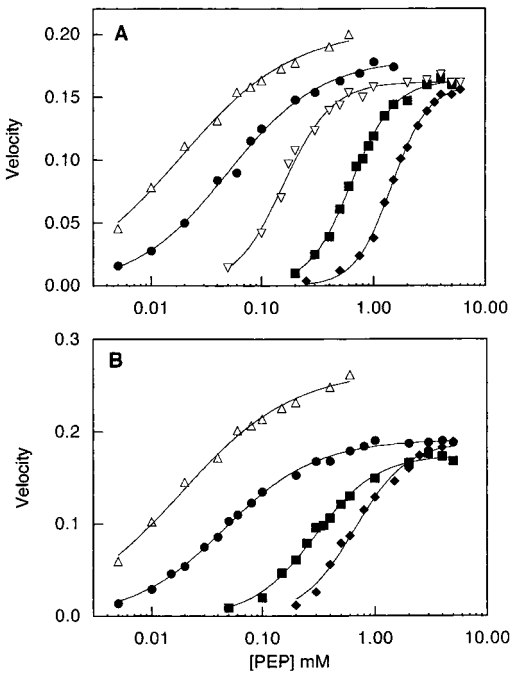

FIGURE 6: Kinetic characterization of S402P RMPK (A) and Y443F RMPK (B) with PEP as the variable substrate. (A) Wild-type RMPK (△); wild-type RKPK (▽); S402P RMPK (●), S402P RMPK in the presence of 12 mM Phe (◆); and S402P RMPK in the presence of both 12 mM Phe and 10 mM FBP (■). Figure 6B: wild-type RMPK (△); Y443F RMPK (●); Y443F RMPK in the presence of 12 mM Phe (◆); and Y443F RMPK in the presence of both 12 mM Phe and 10 mM FBP (■). The ordinate is shown in change in absorbance at 340 nm/min.

Table 4: Kinetic Parameters of RMPK, RKPK, S402P, and Y443F RMPK as a Function of Effectors and PEP as the Variable Substrate

PK	effectors[a]	K_{app} (mM)	n	k_{cat}^s (s^{-1})	$K_{app,I}/K_{app,O}$
WT RMPK	none	0.020 ± 0.002	1.00	253 ± 4	4.4
	I	0.088 ± 0.004	1.8 ± 0.2	249 ± 5	
WT RKPK[b]	none	0.156 ± 0.005	2.1 ± 0.2	200 ± 2	19.4
	I	3.03 ± 0.2	2.3 ± 0.2	192 ± 9	
	I and A	0.078 ± 0.005	1.5 ± 0.1	191 ± 3	
S402P RMPK	none	0.050 ± 0.003	1.0 ± 0.1	223 ± 4	29.2
	I	1.46 ± 0.02	2.6 ± 0.1	197 ± 2	
	I and A	0.63 ± 0.01	2.3 ± 0.1	201 ± 2	
Y443F RMPK	none	0.046 ± 0.001	1.1 ± 0.0	169 ± 1	14.3
	I	0.658 ± 0.031	1.9 ± 0.2	167 ± 4	
	I and A	0.292 ± 0.009	1.6 ± 0.1	154 ± 2	

[a] I is 12 mM Phe, I and A are the combination of both 12 mM Phe and 10 mM FBP, except for RKPK where I is 2 mM Phe, I and A is the combination of both 2 mM Phe and 10 μM FBP. [b] Ref *5*.

Table 5: Kinetic Parameters of the Wild-Type, S402P, and Y443F RMPK with ADP as the Variable Substrate

RMK	K_{app} (mM)	n	k_{cat} (S^{-1})[a]
WT	0.39 ± 0.05	1.3 ± 0.2	288 ± 16
S402P	0.39 ± 0.03	1.0 ± 0.1	236 ± 5
Y443F	0.35 ± 0.02	1.1 ± 0.1	181 ± 3

[a] Values calculated assuming the presence of saturating PEP. The values after the plus or minus (±) sign are the errors obtained upon fitting a particular saturation curve.

In principle, replacing the Tyr with a Phe should only result in a minor change of the side chain, namely the deletion of the hydroxy group (η) which is involved in the hydrogen bond network. In an effort to test this hypothetical mech-

anism with the minimum structural perturbation, it was decided, as an initial attempt to establish the legitimacy of this approach, to mutate Y433 to F to break the intersubunit hydrogen bonding between K421 and Y433.

The CD and sedimentation velocity data indicate that the Y443F mutation does not introduce an observable change in the secondary and quaternary structure of the RMPK enzyme. The effect of the Y443F mutation on the steady-state kinetics is significant (Figure 6, Table 4). In the absence of effectors, the kinetic parameters only show a modest change compared to the wild-type RMPK with the exception of a significant decrease in the catalytic efficiency. In the presence of 12 mM Phe, the apparent affinity for PEP has decreased by 14-fold as compared to a 4-fold decrease for wild-type RMPK (*4*). A perturbation of catalytic efficiency implies that the structural alteration of deleting a hydroxyl group about 30 Å away exherts a long-range effect on the active site. The possible pathway for signal transmission could be explained by the Lys 421 hydrogen binding with Tyr 443, which in turn interacts with the carboxy oxygen of Ala 319, at the C-terminal of the α-helix Aα6. This helix spans the length of a PK subunit. The loop near the N-terminal of this α-helix is part of the PEP-binding site. The replacement of Tyr with a Phe at residue 433 interrupts the molecular linkage between Lys 421 and the active site. As a consequence, the active site could exhibit different catalytic efficiency. Regardless of the specific mechanism, the computation approach adopted in this study can identify the network of interfacial interactions, the significance of which can be tested.

The mechanism of allosteric communication in pyruvate kinase on the basis of 3D structures has been mainly discussed in the framework of domain rotations. Comparing the structure of an inactive T state of the allosteric regulated PK from *E. coli* to the active unregulated structure of mammalian muscle tissues, it was observed that the three domains A, B, and C rotate about 15° within each subunit and the four subunits rotate by about the same amount within the tetramer (*29*, *36*). Specific details of the interfacial region could only be partially compared, as the region corresponding to the Cα1 region was disordered in the *E. coli* crystal structure. It is, however, intriguing that, in the *E. coli* PK structure, which was not used in the modeling, the residue analogous to Lys 421 forms an intrasubunit salt-bridge interaction similar to the predicted alternative conformation in our kidney PK model. These findings suggest a pivotal role of a few residues in coupling a conformational change in the interfacial region to the domain rotations. An intersubunit salt-bridge interaction was also found in the interface between the two α1-loop-α2 regions of the recently determined X-ray crystal structure of the yeast PK (*37*). The residue E395 is conserved among all mammalian yeast PK, but R398 is only conserved among the regulated PK proteins of the M2 type, and is changed to a hydrophobic residue in M1 type. This suggests a conformational change due to different salt-bridge interactions in the allosteric activation.

In summary, this study has demonstrated the usefulness of the software suite DIAMOD/FANTOM for examining alternative conformational states of critical regions of the two PK isozymes. This study identifies the possible role of Lys 421 in intersubunit communication and alternative network of salt bridges that Lys 421 can form with various acidic side chains. This combined approach has also identified two possible ways of breaking the intersubunit interactions involving Lys 421; namely, hydrogen bonding with Tyr 433 and favoring the formation of an alternative salt bridge due to Pro 402. Mutants Y433F and S402P were constructed to test the hypothesis, and the enzymatic kinetic results show that indeed these RMPK mutants have acquired some characteristics that qualitatively resemble RKPK. The results of mutant Y433F further vindicate the conservative approach chosen to test the role of Lys 421 by conducting the minimum structural change instead of the more drastic approach of replacing the functional group of Lys 421, in which case potentially both salt-bridge formation and hydrogen bonding could have been eliminated rendering the interpretation of results more uncertain. The positive effects of mutation in sensitizing the nonallosteric RMPK isozyme to allosteric effectors testify to the value of this combined approach of computational chemistry, genetics, and quantitative functional measurements. The validity of the structural details of the proposed model are forthcoming when the X-ray crystallographic study of the S402P RMPK mutant is completed.

This study presents the initial results of a strategy to elucidate the molecular mechanism of allosteric regulation in mammalian PK. This strategy will now be applied to probe the rationale for the changes in the other 21 residues.

ACKNOWLEDGMENT

A critical reading of the manuscript by Dr. C. H. Schein is appreciated. We thank Dr. Y. Xu for help in preparing Figure 3 and Figure 4.

REFERENCES

1. Larsen, T. M., Laughlin, T., Holden, H. M., Rayment, I., and Reed, G. H. (1994) *Biochemistry 33*, 6301−6309.
2. Muirhead, H., Clayden, D. A., Barford, D., Lorimer, C. G., Fothergill-Gilmore, L. A., Schiltz, E., and Schmitt, W. (1986) *EMBO J. 5*, 475−481.
3. Allen, S. C., & Muirhead, H. (1996) *Acta Crystallogr. 52*, 499−504.
4. Cheng, X., Friesen, R. H. E., and Lee, J. C. (1996) *J. Biol. Chem. 271*, 6313−6321.
5. Friesen, R. H. E., Chin, A., Ledman, D. W., and Lee, J. C. (1998) *Biochemistry 37*, 2949−2960.
6. Consler, T. G., Woodard, S. H., and Lee, J. C. (1989) *Biochemistry 28*, 8756−8764.
7. Noguchi, T., Inoue, H., and Tanaka, T. (1986) *J. Biol. Chem. 261*, 13807−13812.
8. Hall, E. R., and Cottam, G. L. (1978) *Int. J. Biochem. 9*, 785−793.
9. Güntert, P., Braun, W., and Wüthrich, K. (1991) *J. Mol. Biol. 217*, 517−530.
10. Hänggi, G., and Braun, W. (1994) *FEBS Lett. 344*, 147−153.
11. Mumenthaler, C., and Braun, W. (1995) *J. Mol. Mod. 1*, 1−10.
12. Schaumann, T., Braun, W., and Wüthrich, K. (1990) *Biopolymers 29*, 679−694.
13. von Freyberg, B., and Braun, W. (1993) *J. Comput. Chem. 14*, 510−521.
14. von Freyberg, B., and Braun, W. (1991) *J. Comput. Chem. 12*, 1065−1076.
15. Mumenthaler, C., and Braun W. (1995) *Protein Sci. 4*, 863−871.
16. Crick, F. H. C. (1953) *Acta Crystallogr. 6*, 685−689.
17. Kamtekar, S., and Hecht, M. H. (1995) *FASEB J. 9*, 1013−1022.
18. Braun, W. (1987) *Q. Rev. Biophys. 19*, 115−157.
19. Dunbrack, R. L., and Karplus, M. (1994) *Nat. Struct. Biol. 1*, 334−340.

20. Braun, W., and Go, N. (1985) *J. Mol. Biol. 186*, 611−626.
21. Nemethy, G., Pottle, M. S., and Scheraga, H. A. (1983) *J. Phys. Chem. 87*, 1883−1887.
22. Laskowski, R. A., MacArthur, M. W., Moss, D. S., and Thornton, J. M. (1993) *J. Appl. Crystallogr. 26*, 283−291.
23. Sanger, F., Nicklen, S., and Coulson, A. R. (1977) *Proc. Natl. Acad. Sci. U.S.A. 74*, 5463−5467.
24. Boyer, P. D. (1962) *The enzymes* (Boyer, P. D., Lardy, H., and Myrback, K., Eds.) Vol. 6, Academic Press, New York.
25. Bücher, T., and Pfleiderer, G. (1955) *Methods Enzymol. 1*, 435−440.
26. Hill, A. V. (1910) *J. Phys. 40*, 190−224.
27. Laemmli, U. K. (1970) *Nature 227*, 680−685.
28. Morris, A. L., MacArthure, M. W., Hutchinson, E. G., and Thornton, J. M. (1992) *Proteins 12*, 345−364.
29. Mattevi, A., Valentini, G., Rizzi, M., Speranza, M. L., Bolognesi, M., and Coda, A. (1995) *Structure 3*, 729−741.
30. Lesk, A. M. (1991) *Protein Architecture: A Practical Approach*, pp 146−149, IRL Press, Oxford.
31. Fothergil-Gilmore, L. A., and Michels, P. A. M. (1992) *Prog. Biophys. Mol. Biol. 59*, 105−235.
32. Braun, W. (1991) *Computational aspects of the study of macromolecular by NMR* (Hoch, J. C., Pulsen, F. M., and Redfield, C., Eds.) p 199, Plenum Press, New York.
33. Mumenthaler, Ch., Schneider, U., Buchholz, Ch. J., Koller, D., Braun, W., and Cattaneo, R. (1997) *Protein Sci. 6*, 588−597.
34. Buchholz, C. J., Koller, D., Devaux, P., Mumenthaler, Ch., Schneider-Schaulis, J., Braun, W., Gerlier, D., and Cattaneo, R. (1997) *J. Biol. Chem. 272*, 22072−22079.
35. Koradi, R., Billeter, M., and Wüthrich, K. (1996) *J. Mol. Graphics 14*, 51−55.
36. Mattevi, A., Bolognesi, M., and Valentini, G. (1996) *FEBS Lett. 389*, 15−19.
37. Jurica, M. S., Mesecar, A., Heath, P. J., Shi, W., Nowak, T., and Stoddard, B. L. (1998) *Structure 6*, 195−210.

BI981273Y